

Supplemental Material for

Single-layer group III-IV-VI semiconductors: potential photocatalysts for water splitting with high carrier mobilities

Qiu Yang¹, Qi-Dong Hao¹, Cui-E Hu^{2,*}, Hua-Yun Geng³, Xiang-Rong Chen^{1,*}

¹ Institute of Atomic and Molecular Physics, Sichuan University, Chengdu 610065, China;

² College of Physics and Electronic Engineering, Chongqing Normal University, Chongqing 401331, China;

³ National Key Laboratory for Shock Wave and Detonation Physics Research, Institute of Fluid Physics, CAEP, Mianyang 621900, China

Abstract:

As a novel member of two-dimensional (2D) families, the GaGeTe monolayer has been successfully synthesized recently, attracting extensive research attention for its unique physical and chemical properties. However, due to its narrow bandgap, it cannot be applied in photocatalysis. In this work, we have systematically investigated new 2D ternary materials with the chemical formula MSiX (M = Ga, In; X = S, Se, Te) using first-principles calculations. The results show that the stable MSiX monolayers exhibit semiconductor characteristics with band gaps ranging from 1.44 eV to 2.43 eV. GaSiS, GaSiSe, InSiS, and InSiSe can be efficient photocatalysts at pH = 0. By tuning

* Corresponding authors. E-mail: cuiehu@cqnu.edu.cn; xrchen@scu.edu.cn

the pH value, the GaSiTe monolayer exhibits promising photocatalytic activity in a neutral environment. The favorable pH ranges for water splitting of GaSiS, GaSiSe, GaSiTe, InSiS, and InSiSe monolayers are found to be 0-9.5, 0-12.4, 4.1-16.1, 0-6.2, respectively. Biaxial strain tests indicate that these five structures can operate at applicable strain levels (-3% to 3%). All six MSiX monolayers have strong visible-ultraviolet absorption (10^5 cm^{-1}) and high carrier mobilities ($\sim 10^3 \text{ cm}^2 \text{ V}^{-1} \text{ s}^{-1}$). Due to the band degeneracy of VBMs, the effective carrier mobilities of MSiX monolayers were calculated using multi-valley transport theory. These monolayers exhibit high solar-to-hydrogen (STH) efficiency, up to 16.78% at pH = 7 for GaSiS. After stacking, the STH efficiency of the trilayer GaSiS increased to 12.51% at pH = 0. The electron-hole recombination rates were also examined *via* NAMD simulations. Our findings predict that all MSiX monolayers (except for InSiTe) can be potential candidates for photocatalytic water splitting.

Keywords: First-principles calculations; Photocatalytic properties; Optical properties; Carrier mobilities; MSiX monolayers

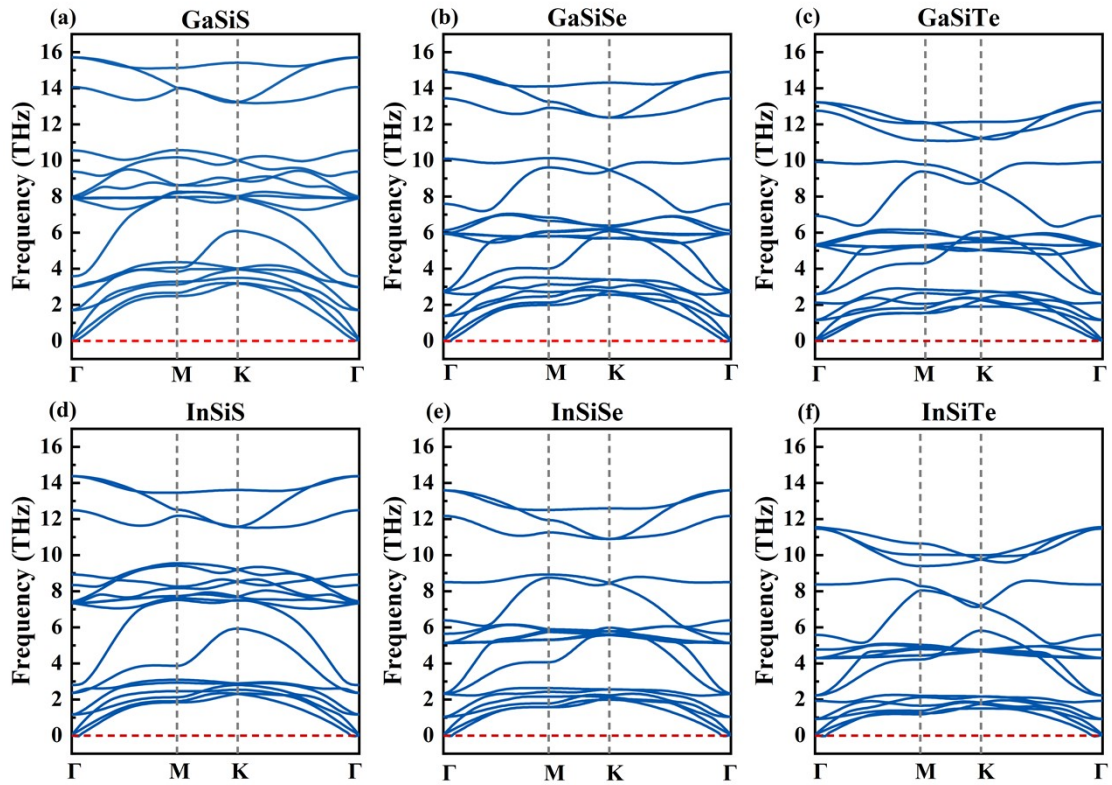


Fig. S1 (Color online) The calculated phonon dispersion curves for MSiX monolayers.

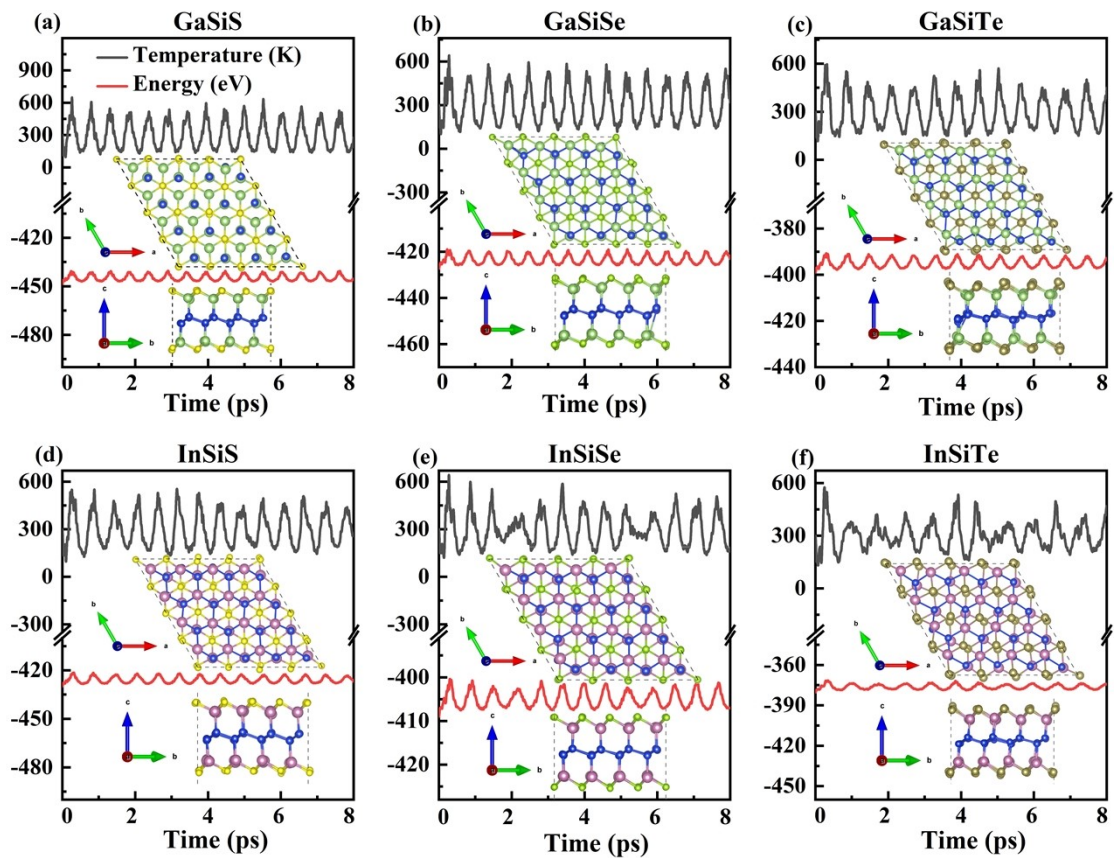


Fig. S2 (Color online) AIMD simulations for MSiX monolayers at 300 K, where the red and black lines represent the variation of the total energy and temperature with time, respectively. The top and side views of the final structures are inserted in the diagrams.

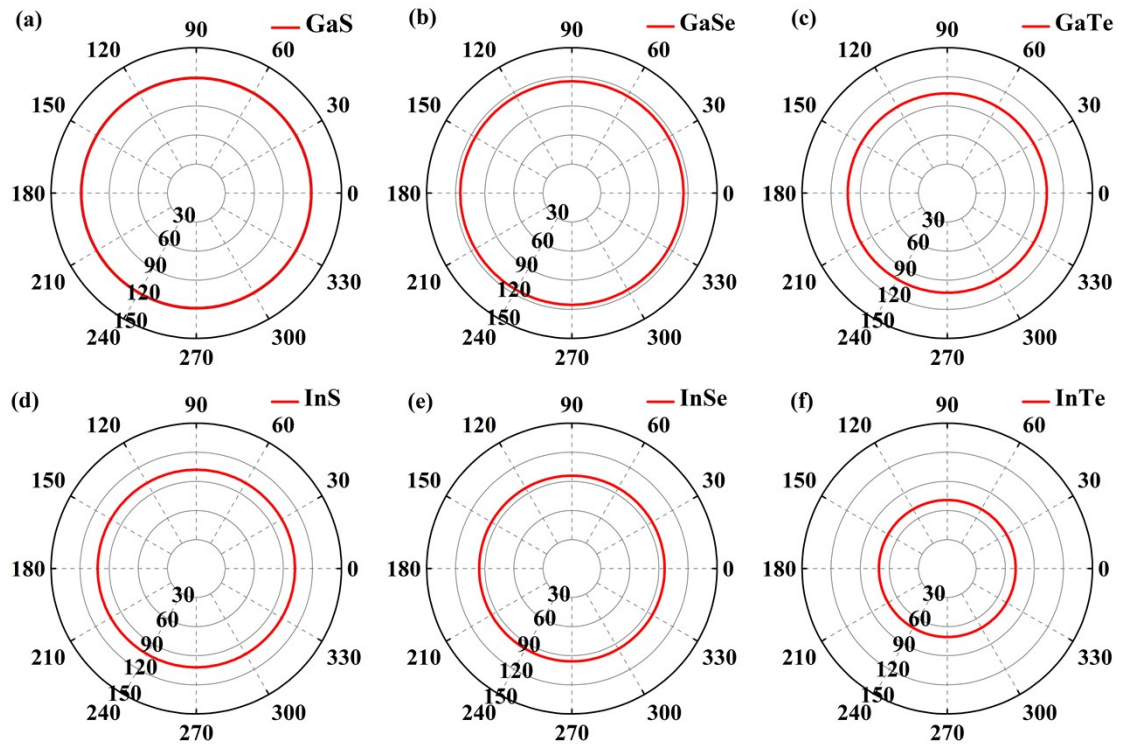


Fig. S3 (Color online) The Young's modulus of 2D MSiX.

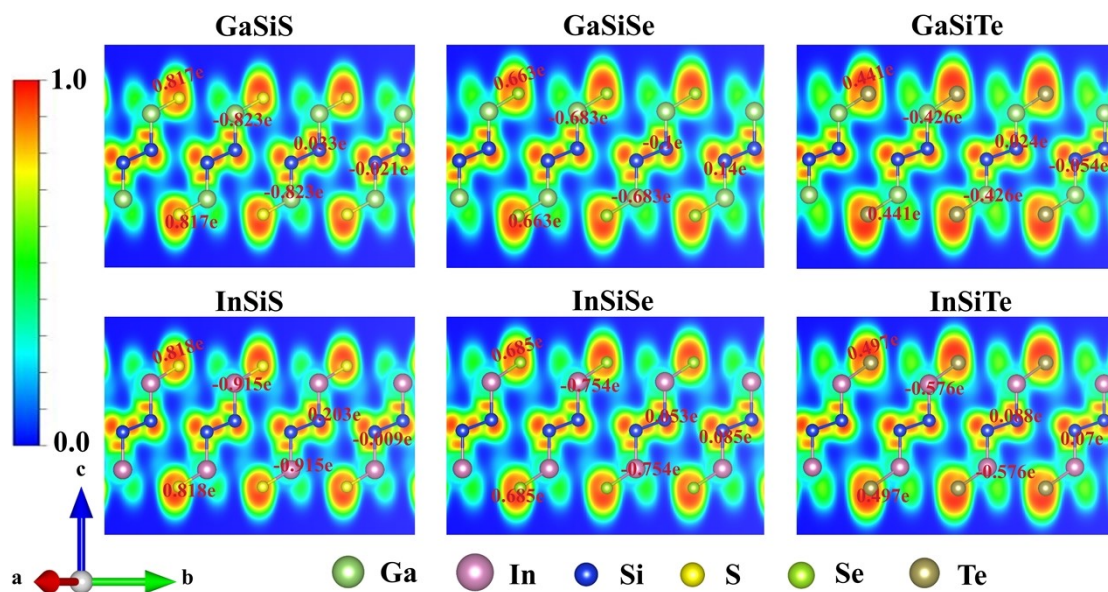


Fig. S4 (Color online) The ELF of MSiX monolayer in the (1 1 0) plane, where the orange-yellow and blue regions represent the electron localization and delocalization, respectively. The gamut bars with values from 0.0 to 1.0 indicate the degree of delocalization of the electrons. The positive and negative values above the atom indicate the gain or loss of electrons.

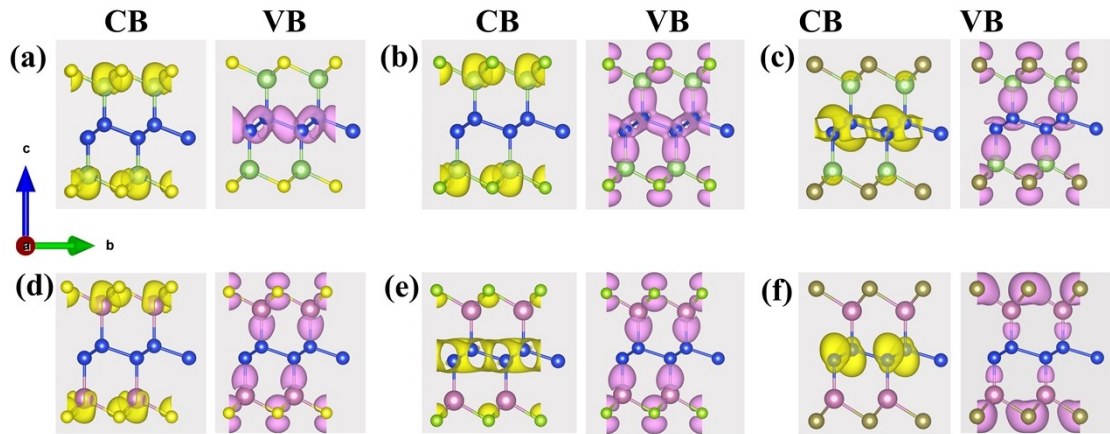


Fig. S5 (Color online) The spatial distribution of the conduction band and valence band for GaSiS (a), GaSiSe (b), GaSiTe (c), InSiS (d), InSiSe (e), and InSiTe (f) monolayers, respectively. The yellow and pink regions indicate the distribution of the conduction and valence bands, respectively.

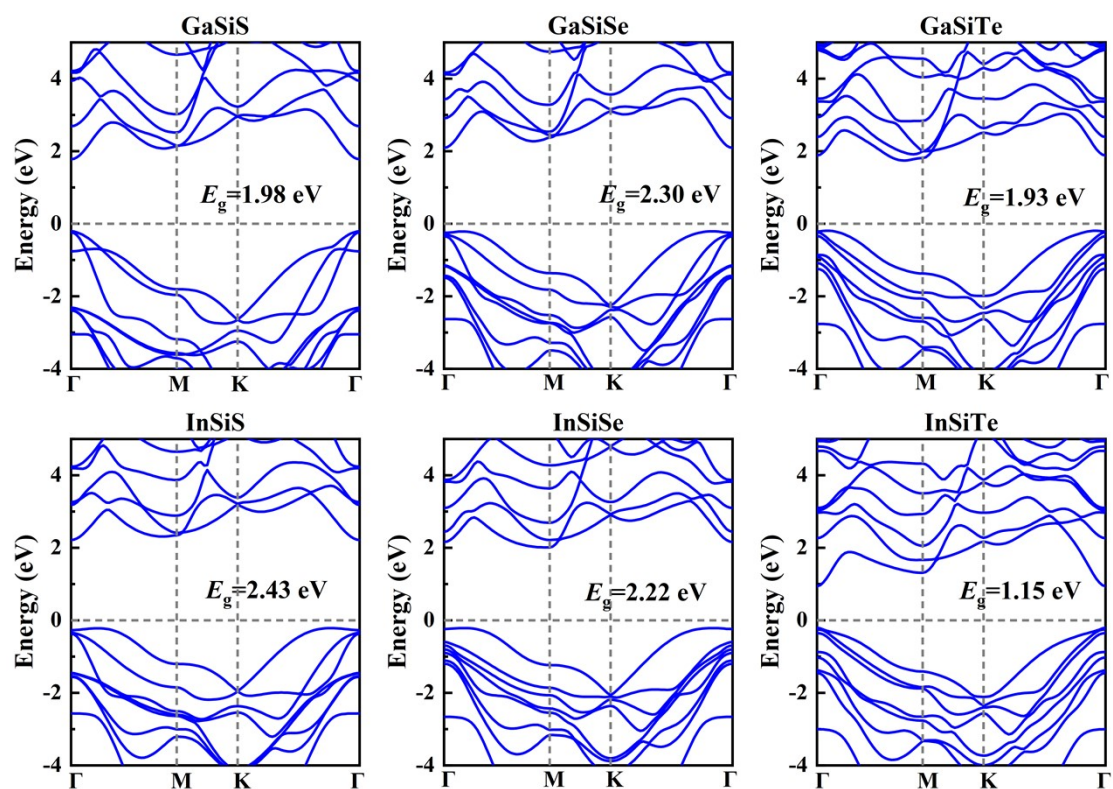


Fig. S6 (Color online) The HSE06 band structure of MSiX monolayers was calculated by considering the SOC effect.

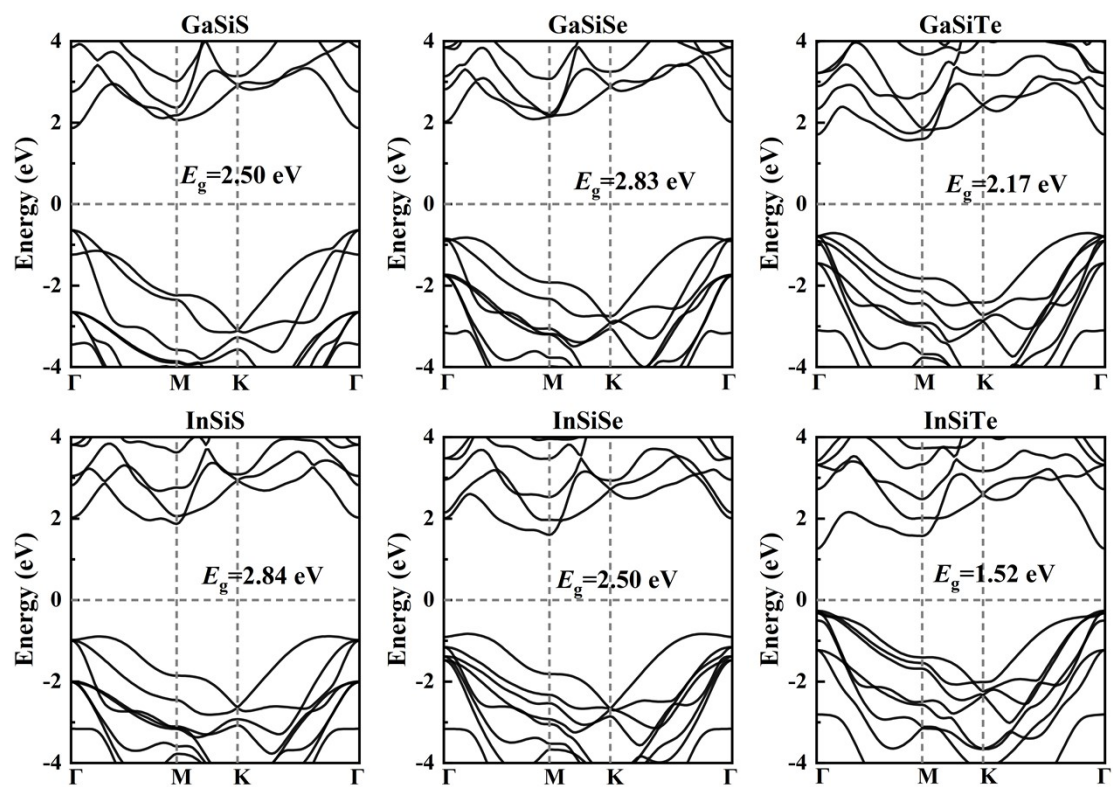


Fig. S7 (Color online) The band structure of MSiX monolayers calculated by the G_0W_0 method.

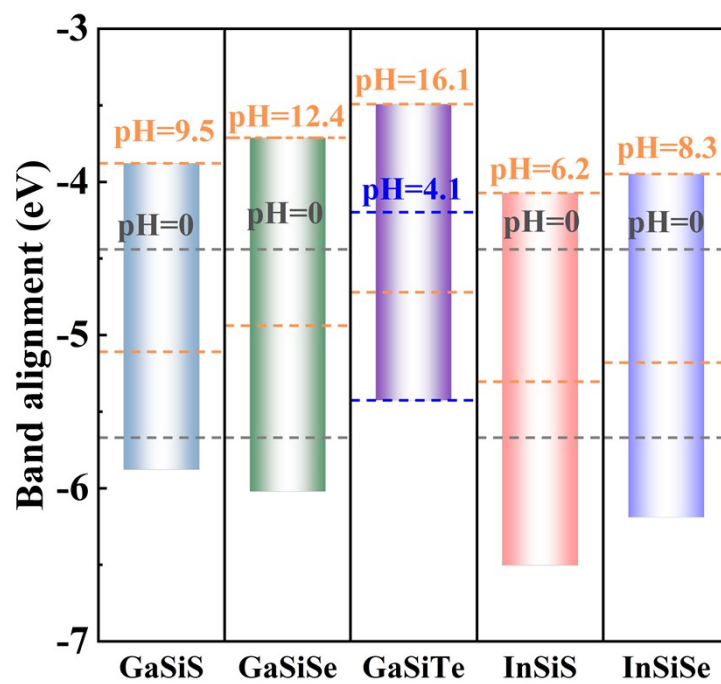


Fig. S8 (Color online) The favorable photocatalytic water splitting pH ranges for MSiX monolayers.

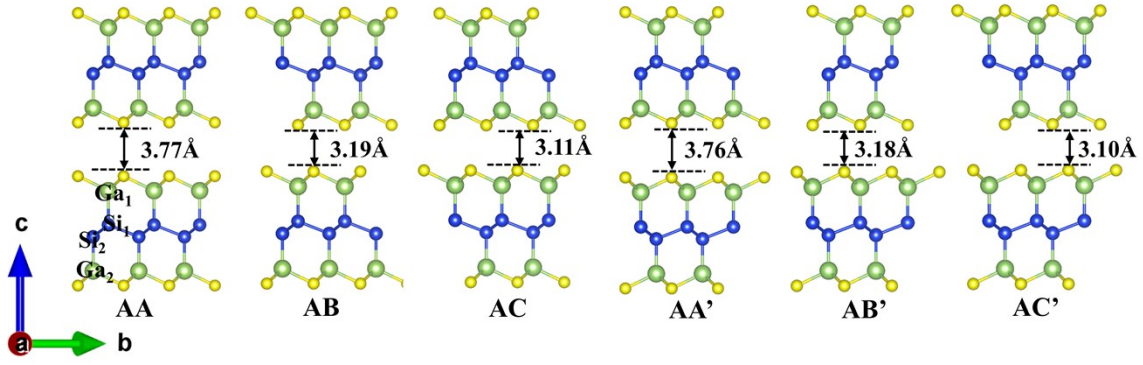


Fig. S9 (Color online) Six high-symmetry stacking types of bilayer Janus GaSiS. For AA, AB, and AC stacking, the two GaSiS are parallelly orientated. S atoms in the upper layer are located at the S-top site (AA), the Ga₁/Si₁-top site (AB), and the Ga₂/Si₂-top site (AC) in the lower layer. For AA', AB', and AC' stacking, the two GaSiS monolayers are antiparallely orientated. S atoms in the upper layer are settled on the S-top site (AA'), the Ga₁/Si₁-top site (AB'), and the Ga₂/Si₂-top site (AC') in the lower layer.

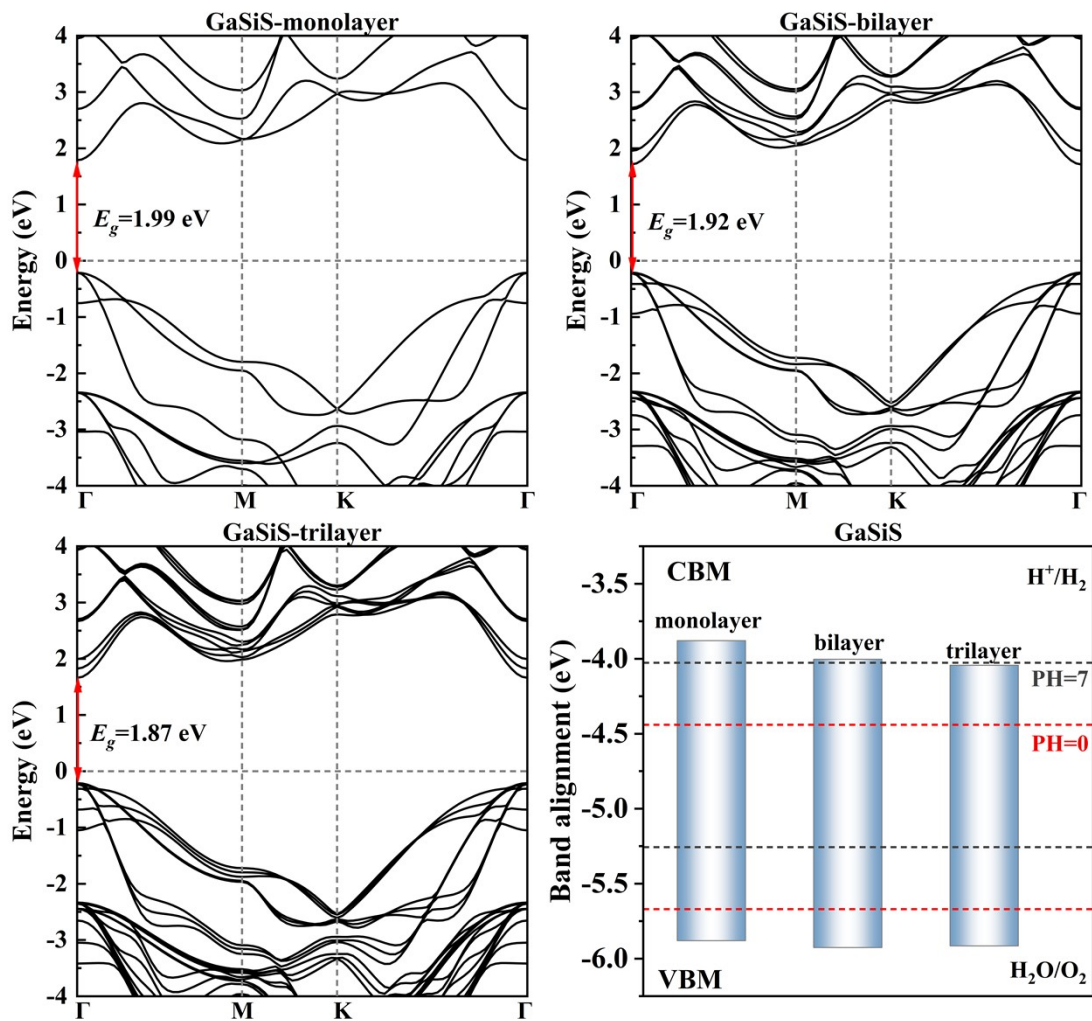


Fig. S10 (Color online) Band structures for monolayer GaSiS (a), bilayer GaSiS (b), and trilayer GaSiS (c) at the HSE06 method. Band alignment for GaSiS with different layers (d).

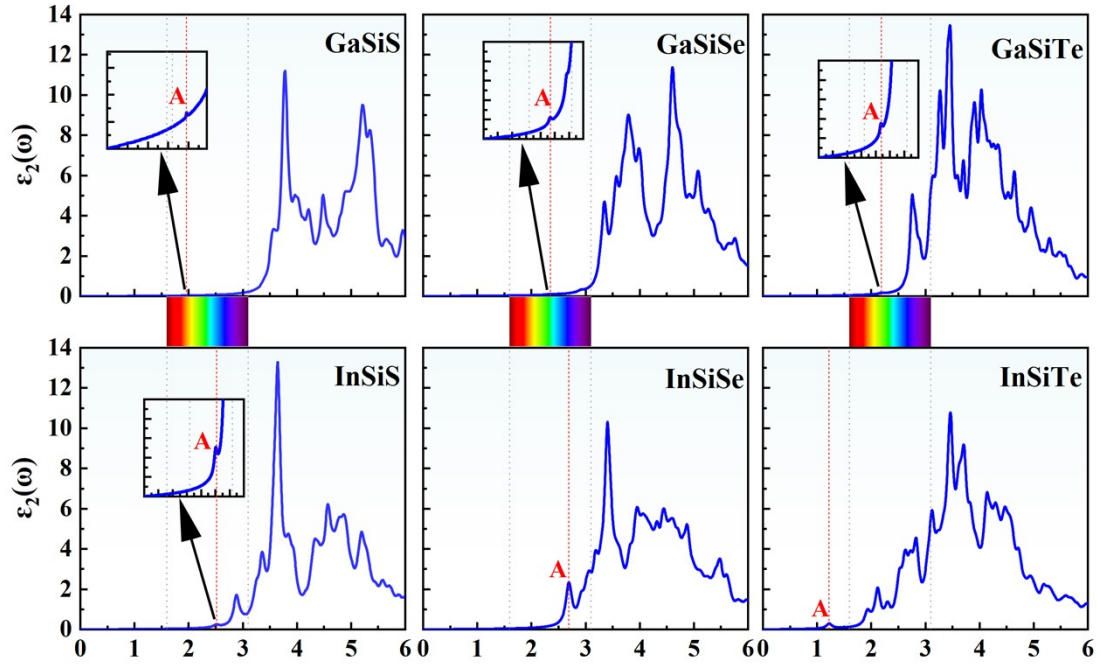


Fig. S11 (Color online) The imaginary parts of the dielectric function are calculated using the $G_0W_0 + BSE$ method for MSiX monolayers.

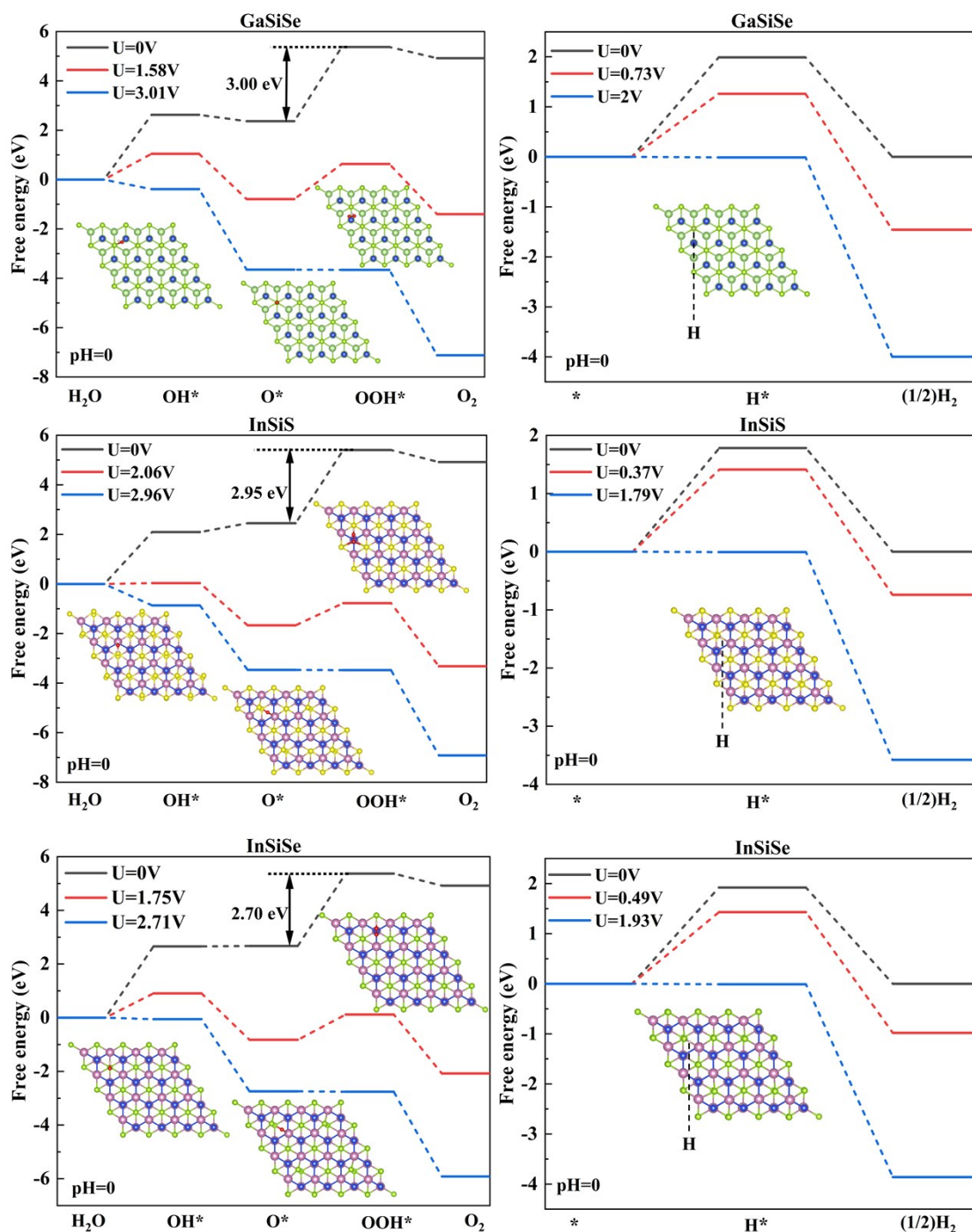


Fig. S12 (Color online) The free energy steps and proposed photocatalytic pathways of oxygen evolution reaction (OER) (left) and hydrogen evolution reaction (HER) (right) under pH = 0 conditions for GaSiSe, InSiS, and InSiSe monolayers.

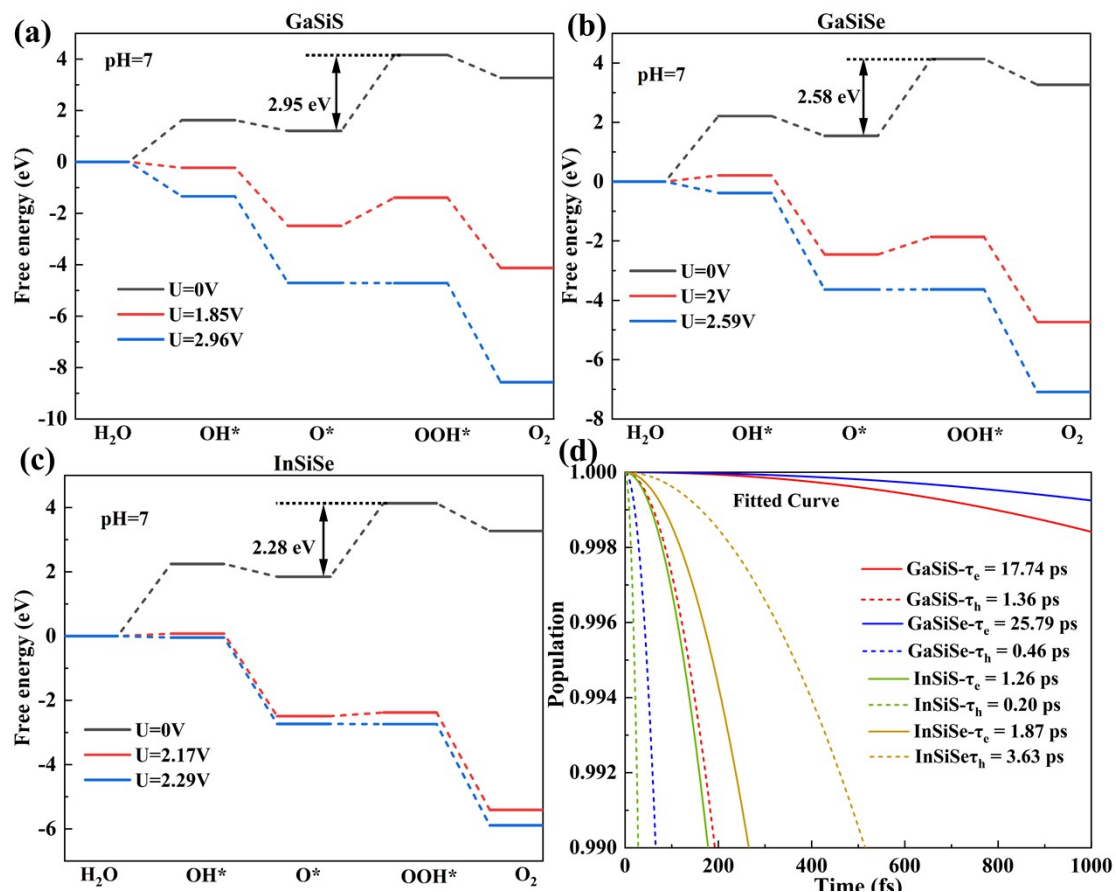


Fig. S13 (Color online) (a-c) The free energy steps and proposed photocatalytic pathways of oxygen evolution reaction (OER) under pH = 7 for GaSiS, GaSiSe, and InSiSe monolayers. (d) The electrons and holes dynamics of 2D MSiX monolayer.

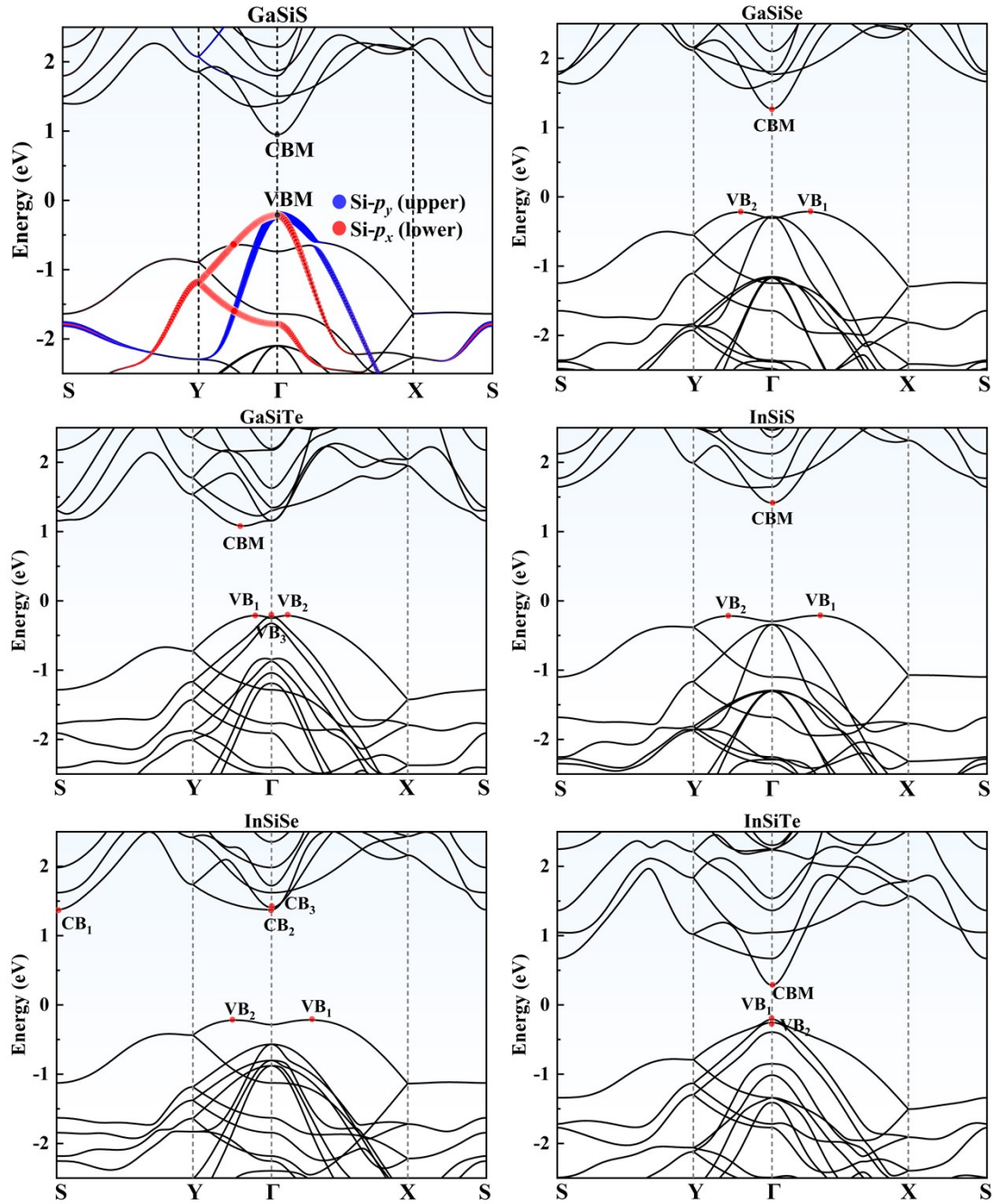


Fig. S14 (Color online) The electronic structure of the MSiX monolayers based on the orthorhombic cell at the PBE level (PBE+SOC level for GaSiTe and InSiTe). VB₁, VB₂, and VB₃ refer to the highest, second-highest, and third-highest valence band extrema, respectively. CB₁, CB₂, and CB₃ represent the lowest, second-lowest, and third-lowest conduction band extrema, respectively.

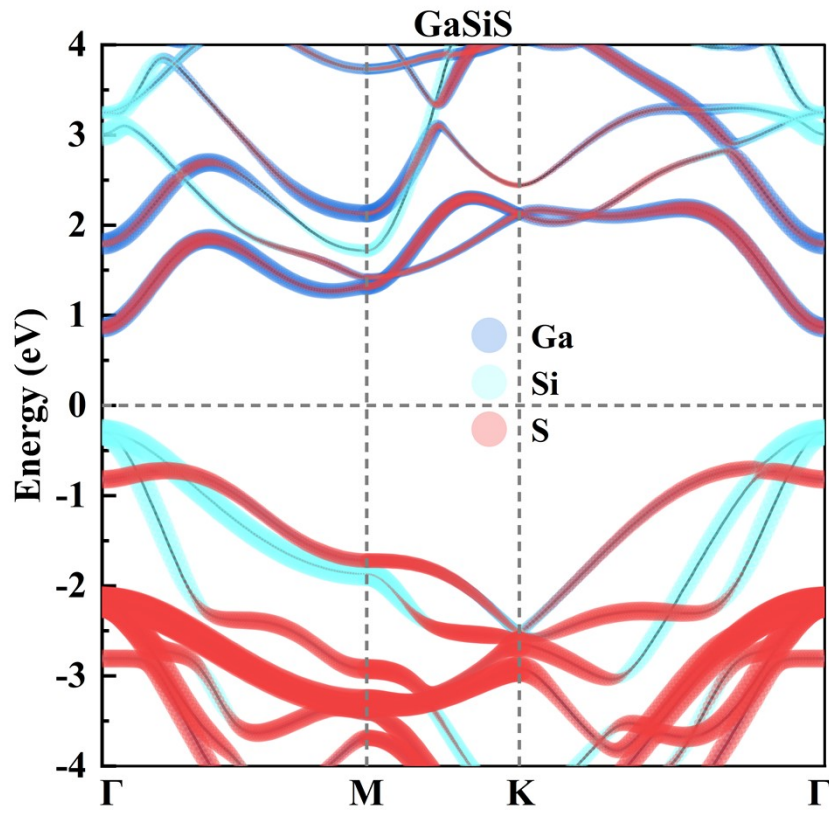


Fig. S15 (Color online) The projected band structures of the GaSiS monolayer calculated by the PBE functional.

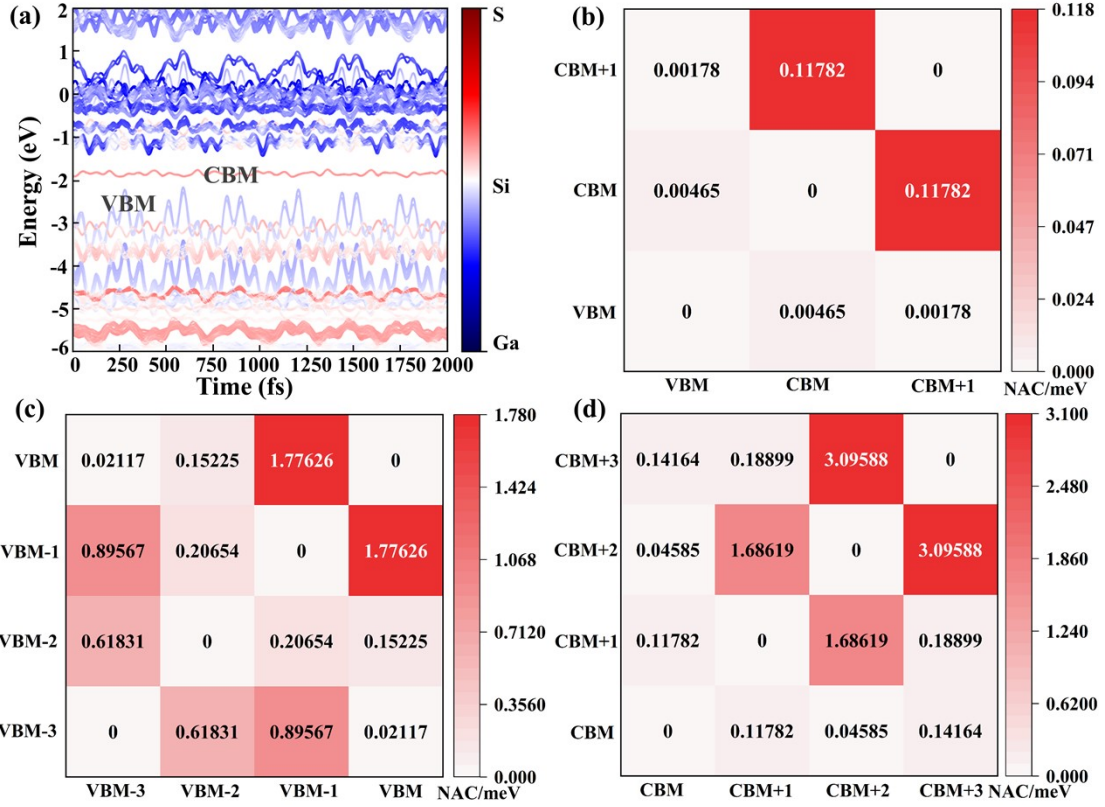


Fig. S16 (Color online) (a) The energy evolution of Kohn-Sham (KS) states of GaSiS monolayer near the Fermi level at 300 K. (b-c) The time-averaged absolute values of non-adiabatic coupling (NAC) between different states for GaSiS monolayer. The color bar in the NAC heatmap indicates the strength of the interaction.

Table S1 The overpotential for HER $\chi(\text{H}_2)$ and overpotential for OER $\chi(\text{O}_2)$, as well as the predicted efficiency of light absorption (η_{abs}), carrier utilization (η_{cu}), and solar-to-hydrogen (η_{STH}) of MSiX (M = Ga, In; X = S, Se) at pH = 0 (in brackets: at pH = 7). nL (n = 1 to 3) represents different layers.

Material	Strain (%)	$\chi(\text{H}_2)$ (eV)	$\chi(\text{O}_2)$ (eV)	η_{abs} (%)	η_{cu} (%)	η_{STH} (%)
GaSiS(1L)	0	0.55 (0.14)	0.21 (0.62)	37.02 (37.02)	25.79 (45.34)	9.55 (16.78)
	-3	0.05 (-0.36)	0.58 (0.99)	43.20 (--)	39.68 (--)	17.14 (--)
GaSiS(2L)	0	0.44 (0.02)	0.26 (0.67)	40.16 (40.16)	29.04 (38.33)	11.66 (15.39)
GaSiS(3L)	0	0.40 (-0.02)	0.24 (0.66)	42.63 (--)	29.34 (--)	12.51 (--)
GaSiSe(1L)	0	0.73 (0.32)	0.35 (0.76)	24.21 (24.21)	27.84 (44.78)	6.74 (10.84)
	-3	0.17 (-0.25)	0.28 (0.69)	52.59 (--)	32.6 (--)	17.14 (--)
GaSiTe(1L)	0	(0.54)	(0.17)	(39.72)	(24.64)	(9.79)
	-3	(0.04)	(0.16)	(65.48)	(26.17)	(17.14)
InSiS(1L)	0	0.37 (-0.05)	0.83 (0.83)	20.10 (--)	43.32 (--)	8.71 (--)
	-3	0.04 (-0.37)	0.64 (1.05)	40.86 (--)	39.36 (--)	16.08 (--)
InSiSe(1L)	0	0.50 (0.09)	0.51 (0.92)	26.81 (26.81)	38.92 (37.67)	10.44 (10.10)
	-3	0.12 (-0.29)	0.36 (0.77)	45.86 (--)	31.88 (--)	14.62 (--)

Table S2 The interlayer distance, and binding energy of the bilayer GaSiS with different stacking orders. The interlayer binding energy E_b with the expression $E_b = (nE_1 - E_n)/(nA)$.

Pattern	AA	AB	AC	AA'	AB'	AC'
d (Å)	3.77	3.19	3.11	3.76	3.18	3.10
E_b (meV/Å ²)	11.52	16.81	16.63	11.44	16.83	16.89

Table S3 The calculated indirect QP band gaps E_g^i (QP), direct QP band gaps E_g^d (QP), first excitonic energies (optical gaps) E_1 , and exciton binding energies E_b of MSiX monolayers. All the values are in eV.

	E_g^i (QP)	E_g^d (QP)	E_1	E_b
GaSiS	2.50	2.50	1.95	0.55
GaSiSe	2.83	2.86	2.35	0.51
GaSiTe	2.17	2.52	2.19	0.33
InSiS	2.83	3.00	2.52	0.49
InSiSe	2.50	2.91	2.68	0.23
InSiTe	1.52	1.52	1.22	0.30

Table S4 Elastic modulus (C_{2D}), effective mass (m^*), deformation potential (E_1), and carrier mobility (μ_{2D}) for GaSiSe monolayers along the x and y direction at the PBE level. The carrier mobility computed using the Lang-Zhang-Liu anisotropic method is displayed in the brackets.

Materials	Carrier types		C_{2D} (Nm ⁻¹)	m^* (m_e)	E_1 (eV)	μ_{2D} (cm ² V ⁻¹ s ⁻¹)
GaSiSe	Electrons	x	122.60	0.154	-8.83	1413.14 (1410.14)
		y	122.28	0.154	-8.84	1405.17 (1408.15)
	Holes (VB ₁)	x	122.60	1.200	1.19	849.73 (648.04)
		y	122.283	2.728	1.64	197.00 (243.42)
	Holes (VB ₂)	x	122.60	2.252	1.69	235.54 (286.81)
		y	122.28	1.307	1.26	733.08 (571.79)

Table S5 Elastic modulus (C_{2D}), effective mass (m^*), deformation potential (E_1), and carrier mobility (μ_{2D}) for GaSiTe monolayers along the x and y direction at the PBE + SOC level. The carrier mobility computed using the Lang-Zhang-Liu anisotropic method is displayed in the brackets.

Materials	Carrier types		C_{2D} (Nm ⁻¹)	m^* (m_e)	E_1 (eV)	μ_{2D} (cm ² V ⁻¹ s ⁻¹)
GaSiTe	Electrons	x	108.79	0.194	-5.16	1448.80 (2028.66)
		y	108.84	0.496	2.94	1748.78 (1040.31)
	Holes (VB ₁)	x	108.79	2.804	-1.35	330.28 (660.85)
		y	108.84	0.670	-0.18	78891.67 (5442.08)
	Holes (VB ₂)	x	108.79	0.653	-0.29	29767.87 (5556.90)
		y	108.84	2.824	-1.23	398.51 (730.02)
	Holes (VB ₃)	x	108.79	0.446	-6.51	270.86 (269.97)
		y	108.84	0.459	-6.54	260.91 (261.76)

Table S6 Elastic modulus (C_{2D}), effective mass (m^*), deformation potential (E_1), and carrier mobility (μ_{2D}) for InSiS monolayers along the x and y direction at the PBE level. The carrier mobility computed using the Lang-Zhang-Liu anisotropic method is displayed in the brackets.

Materials	Carrier types		C_{2D} (Nm ⁻¹)	m^* (m_e)	E_1 (eV)	μ_{2D} (cm ² V ⁻¹ s ⁻¹)
InSiS	Electrons	x	110.26	0.242	-5.17	1498.24 (1515.30)
		y	109.89	0.242	-5.09	1544.52 (1526.87)
	Holes (VB ₁)	x	110.26	1.666	-1.666	76.28 (58.96)
		y	109.89	5.076	-5.076	13.57 (16.64)
	Holes (VB ₂)	x	110.26	3.779	-3.779	22.71 (25.53)
		y	109.89	1.731	-1.731	69.25 (60.58)

Table S7 Elastic modulus (C_{2D}), effective mass (m^*), deformation potential (E_1), and carrier mobility (μ_{2D}) for InSiSe monolayers along the x and y direction at the PBE level. The carrier mobility computed using the Lang-Zhang-Liu anisotropic method is displayed in the brackets.

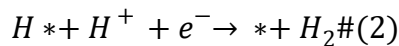
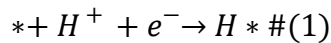
Materials	Carrier types		C_{2D} (Nm ⁻¹)	m^* (m_e)	E_1 (eV)	μ_{2D} (cm ² V ⁻¹ s ⁻¹)
InSiSe	Electrons (CB ₁)	x	103.30	0.428	0.51	75053.35 (1939.18)
		y	100.70	0.161	-6.60	1165.80 (2461.00)
	Electrons (CB ₂)	x	103.30	0.123	-9.94	326.00 (508.38)
		y	100.70	2.511	4.23	85.93 (36.51)
	Electrons (CB ₃)	x	103.30	0.170	-6.73	1682.20 (1720.30)
		y	100.70	0.170	-6.44	1787.97 (1746.72)
	Holes (VB ₁)	x	103.30	1.748	2.20	84.90 (67.15)
		y	100.70	5.345	2.89	15.75 (19.08)
	Holes (VB ₂)	x	103.30	4.637	2.86	19.95 (22.96)
		y	100.70	1.827	2.30	76.37 (64.54)

Table S8 Elastic modulus (C_{2D}), effective mass (m^*), deformation potential (E_1), and carrier mobility (μ_{2D}) for InSiTe monolayers along the x and y direction at the PBE + SOC level. The carrier mobility computed using the Lang-Zhang-Liu anisotropic method is displayed in the brackets.

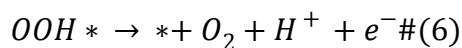
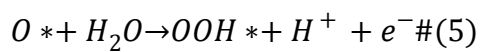
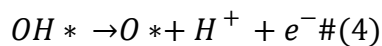
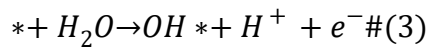
Materials	Carrier types		C_{2D} (Nm ⁻¹)	m^* (m_e)	E_1 (eV)	μ_{2D} (cm ² V ⁻¹ s ⁻¹)
InSiTe	Electrons	x	80.87	0.094	-9.33	2240.39 (2413.69)
		y	81.04	0.094	-8.42	2755.05 (2541.56)
	Holes (VB ₁)	x	80.87	0.173	-5.88	1663.85 (1665.93)
		y	81.04	0.173	-5.88	1669.40 (1667.32)
	Holes (VB ₂)	x	80.87	0.333	-6.07	421.54 (421.81)
		y	81.04	0.333	-6.07	422.27 (422.00)

Calculation details of the free energy change (ΔG) for MSiX monolayers

The hydrogen production reaction (HER) proceeds in the following two steps:



Meanwhile, the oxygen evolution reaction (OER) consists of four steps, which can be written as:



where * indicates the adsorbed materials, and *A refers to the adsorbed intermediates on materials surface.

As mentioned in the main text, the free energy change (ΔG) is defined as: $\Delta G = \Delta E + \Delta E_{ZPE} - T\Delta S + \Delta G_U + \Delta G_{PH}$ proposed by Norskov *et al.* Accordingly, the free energy difference under the effect of pH and an extra potential bias for each reaction of both hydrogen and oxidation production can be expressed as follows:

$$\Delta G_1 = G_{H^*} - \frac{1}{2}G_{H_2} - G_{H^*} + \Delta G_U + \Delta G_{PH} \#(7)$$

$$\Delta G_2 = G_{H^*} + \frac{1}{2}G_{H_2} - G_{H^*} + \Delta G_U + \Delta G_{PH} \#(8)$$

$$\Delta G_3 = G_{OH^*} + \frac{1}{2}G_{H_2} - G_{H^*} - G_{H_2O} + \Delta G_U - \Delta G_{PH} \#(9)$$

$$\Delta G_4 = G_{O^*} + \frac{1}{2}G_{H_2} - G_{OH^*} + \Delta G_U - \Delta G_{PH} \#(10)$$

$$\Delta G_5 = G_{OOH^*} + \frac{1}{2}G_{H_2} - G_{O^*} - G_{H_2O} + \Delta G_U - \Delta G_{PH} \#(11)$$

$$\Delta G_6 = G_{H^*} + \frac{1}{2}G_{H_2} + G_{O^*} - G_{OOH^*} + \Delta G_U - \Delta G_{PH} \#(12)$$

The intermediate steps are estimated by simulating the intermediate adsorption on a $2 \times 2 \times 1$ supercell of the MSiX monolayers. To find the most favorable surface active site, we opted for different adsorption sites, including positions directly above the S/Se atom, directly above the Ga/In atom, above the S/Se-Ga/In bond, near the center of the hexagonal lattice, and others. Then we selected the adsorption model with the lowest and most stable energy.